https://doi.org/10.1016/j.sna.2020.112031

Design and performance enhancement of a force-amplified piezoelectric stack energy harvester under pressure fluctuations in hydraulic pipeline systems

Dong-Xing Cao † [1,2], Xiang-Jian Duan[1,2], Xiang-Ying Guo[1,2], Siu-Kai Lai[3]

[1] College of Mechanical Engineering, Beijing University of Technology, Beijing 100124, China

[2] Beijing Key Laboratory of Nonlinear Vibrations and Strength of Mechanical Structures, Beijing 100124, China

[3] Department of Civil and Environmental Engineering, The Hong Kong Polytechnic University, Hung Hom, Kowloon, Hong Kong, China

Abstract: Pipelines are a safe and environmentally friendly way to convey fluids over a long distance. Pressure fluctuations generated by unsteady flows are a common phenomenon in hydraulic pipeline systems. In this paper, a piezoelectric stack energy harvester is designed to scavenge the vibration energy of pressure fluctuations in pipeline systems, where a force amplifier is introduced as an auxiliary booster to enhance the energy conversion efficiency under low-frequency excitation levels. The device can be integrated with health monitoring sensors to eliminate the needs of batteries or wired power supplies to individual sensors. The working principle of the force amplifier is analyzed by investigating the magnification coefficient based on a dynamic model. The optimized structural parameters are also investigated by theoretical studies. Besides, the finite element model of the force amplifier is also constructed to analyze the magnification coefficient and to validate the theoretical results. Experimental studies are also carried out to identify the effect of the force amplifier on the proposed energy harvester. The results show that there is great potential to realize a self-powered wireless sensor network technology for pipeline monitoring.

Keywords: Vibration energy harvesting, Pressure fluctuation, Force amplifier, Piezoelectric stack, Hydraulic pressure pipeline system

† Corresponding author, E-mail: caostar@bjut.edu.cn

1. Introduction

With the advancement of microelectronic technologies, the necessity of autonomous power sources for low-power electronic devices has attracted much attention. Vibration-based energy harvesting (VEH) techniques, which can transform ambient mechanical energy from external sources to electric energy, is an ideal solution to drive small-scale and wireless devices, like those used in wearable electronics and wireless sensors. In recent years, a plenty of research studies have devoted great efforts on different technologies of VEH, and various transduction mechanisms have been used, such as electrostatic [1-3], electromagnetic [4-6], piezoelectric [7-11] and ferroelectric approaches [12-15]. On the other hand, many structure forms have been proposed to improve and enhance the performance of vibration energy harvesters, including bi-stable [16-18], multi-stable [19-22] and multi-degree models [23-25]. There are some studies to investigate various types of vibration energy harvesters under stochastic excitations [26, 27], nonlinear internal resonance effects [28-31] and flow-induced sources [32, 33].

For vibration energy harvesters, one of the key points is the excitation source, which can affect the design and effectiveness of VEH. In reality, ambient sources are often low-frequency and low-amplitude in nature. Many research studies mainly focused on base excitations (or foundation excitations). In industrial engineering fields, pipeline transport is the long-distance transportation of fluids through a system of pipes. Pressure fluctuations are a common phenomenon due to unsteady flows in hydraulic pipeline systems. In this aspect, Cunefare et al. [34, 35] proposed a hydraulic pressure energy harvester to convert mechanical energy induced by pressure fluctuations in high-pressure hydraulic pipelines into electrical energy. Pressure fluctuations in water pipeline systems are generally weak. In order to capture more energy under low pressure, the structure of this harvester needs to be further optimized. However, only a few studies have attempted to enhance the working efficiency of VEH techniques on hydraulic pipeline systems.

Force amplifiers that can magnify excitation forces have been introduced to VEH techniques to improve the energy conversion efficiency. For example, Feenstra et al. [36] proposed an energy harvesting backpack, using a mechanically amplified piezoelectric stack, with a mean power output from the energy harvester of approximately 0.4 mW. An optimal

design of the force magnification frame for a piezoelectric stack energy harvester was also studied by Chen et al. [37], who found that the tilt angle and thickness of beams used for force magnification are two major factors that can significantly affect the energy conversion efficiency. Wang et al. [38] presented the theoretical model and experimental validation of a piezoelectric stack energy harvester with a flexure free convex force amplification frame to convert walking force into electricity. In addition, Kuang et al. [39] designed a sandwiched piezoelectric transducer for energy harvesting in large force environment. Qian et al. [40] adopted a force amplification frame to transmit and amplify the vertical heel-strike force to the inner piezoelectric stack that can be used as an embedded piezoelectric footwear harvester. Furthermore, Evans et al. [41] investigated a force amplified piezoelectric stack device that was found to have a maximum level of amplification at low-frequency levels, this study signified its applicability for low-frequency energy harvesting. More recently, Keshmiri et al. [42] also proposed a new analytical model for a composite energy harvester with embedded piezoelectric stacks using the pure in-plane polarization. The results showed that a higher conversion efficiency can be achieved when comparing with a conventional unimorph harvester with identical geometrical and material properties.

In this work, an enhanced pressure fluctuation energy harvester (PFEH) is designed for energy harvesting from a hydraulic pressure pipeline system, which can be integrated with monitoring sensors without the needs of batteries and wired power supplies to individual sensors. This present study mainly focuses on the pressure fluctuation of water pipelines in real-life applications as a low-frequency excitation source for energy harvesting. First, a force amplifier [43] is designed and optimized to enhance the conversion efficiency. The working principle of the force amplifier is analyzed by using a dynamic model. To study the dynamic characteristics of this system, the open-circuit voltage of the enhanced PFEH under various case scenarios is presented. The optimized structural parameters of the force amplifier, which can improve the open-circuit voltage of the enhanced PFEH, are determined by a theoretical analysis. Furthermore, both finite element and experimental studies are conducted to verify the correctness of the theoretical model. Finally, important findings of this work are summarized.

2. Theoretical model analysis

2.1 Mechanical structure of the enhanced PFEH

A new type of the PFEH is designed to harness hydraulic energy in fluids within a pumped-fluid system and turn into usable electrical energy, which can then be used to power sensor nodes or low-power devices. An illustrative diagram of the enhanced PFEH is shown in Figure 1. Consider a hydraulic pressure pipeline where pressure fluctuations are an excitation source for this energy harvester. Another important component is a force amplifier, where the piezoelectric stack is fixed to realize an electromechanical transformation. In the figure, an interface film is used to separate the fluid flow from the force amplifier. Indeed, this interface is a fluid-mechanical coupling between the force amplifier and the pressure fluctuation. The force amplifier can be excited by pressure fluctuations, this is also referred as pressure ripples.

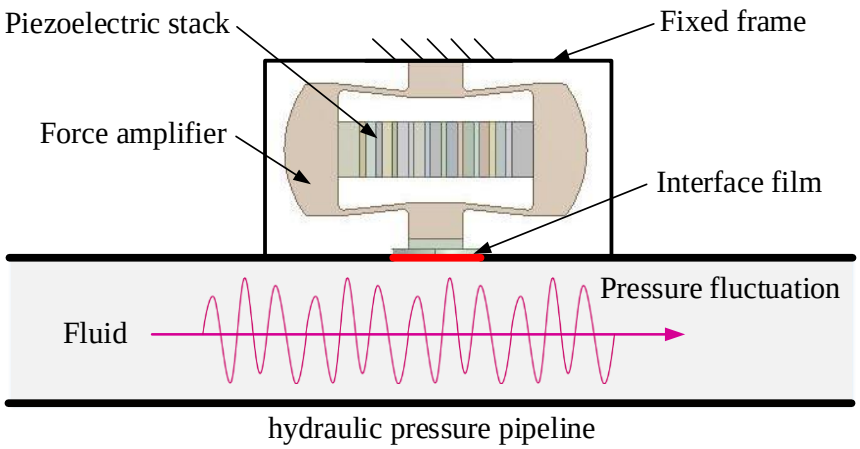

Figure 1. Schematic of the enhanced PFEH

2.2 Dynamic model of PFEH

2.2.1 Amplification factor of the force amplifier

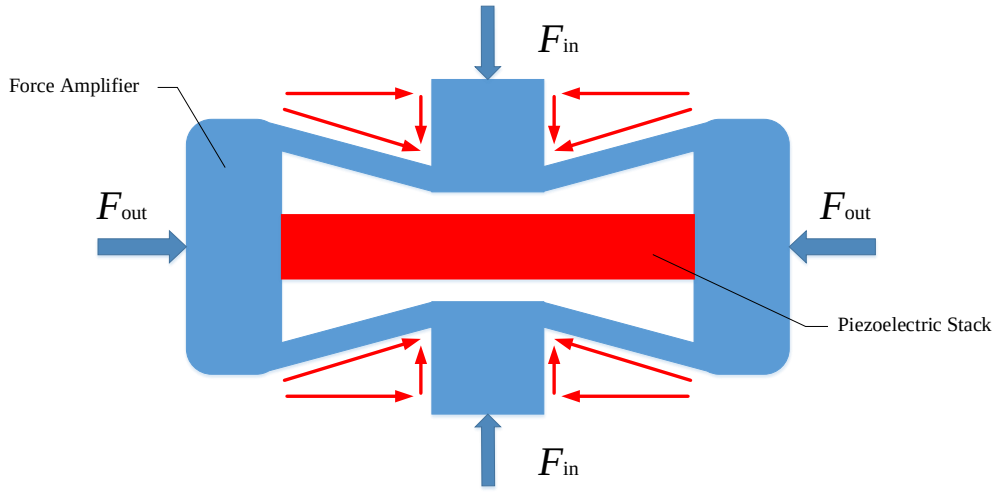

Figure 2. A force analysis diagram of the force amplifier

The force amplifier is used to amplify external excitation forces that act on the piezoelectric stack. The working principle of the force amplifier is illustrated by a dynamic model, as shown in Figure 2. According to Newton's law, when an external excitation (F_{in}) exerts on the force amplifier, the piezoelectric stack will be subjected to an elastic excitation (F_{out}) due to the elastic deformation of the force amplifier. Based on the geometric relationship, we have [43]

$$F_{out} = F_{in}\cot\theta \tag{1}$$

where θ is the angle of each of the four beams with respect to the horizontal direction, i.e., structural angle. With the increase of excitation frequency, the resonant phenomenon will occur, Eq. (1) is thus not applicable. Due to this reason, the dynamic model of the force amplifier is required to be further analyzed when the elastic excitation F_{out} is under a resonant condition. It is assumed that the structure of the mechanical amplifier is completely symmetric, and the external excitation force transmitted to the two ends of the piezoelectric stack is the same and uniformly distributed. Because of the structural symmetry, a quarter model is only considered for dynamic analysis, as shown in Figure 3. It is clear that the deformation of the force amplifier mainly occurs in the beam parts that can be regarded as a cantilever. Other parts can be regarded as a rigid body. Assume that only bending deformation will occur in the beam parts, the governing equation of the beams can be established by using a spring-mass system with equivalent stiffness and mass (see Figure 3(c)) as follows:

$$m_L\ddot{x} + C_L\dot{x} + K_L x = \frac{1}{2}F_{in}cos\theta \tag{2}$$

where $m_L = \frac{33}{140}m_1 + m_2$, $K_L = \frac{3E_L J}{l^3}$, $J = \frac{bh^3}{12}$, and $F_{in} = F_0 sin\omega t$. Here, m_L and K_L are the equivalent mass and stiffness of the cantilever beam, respectively. F_0 and ω are the amplitude and frequency of external excitations, respectively. In addition, C_L is a damping coefficient, E_L is the elastic modulus of the cantilever beam, J is the moment of inertia of the cantilever beam, m_1 is the mass of the cantilever beam, m_2 is the mass of the counterpart in contact with the vibration source, l is the length of the cantilever beam, b is the breadth of the cross-section of the cantilever beam, and h is the height of the cross-section of the cantilever beam.

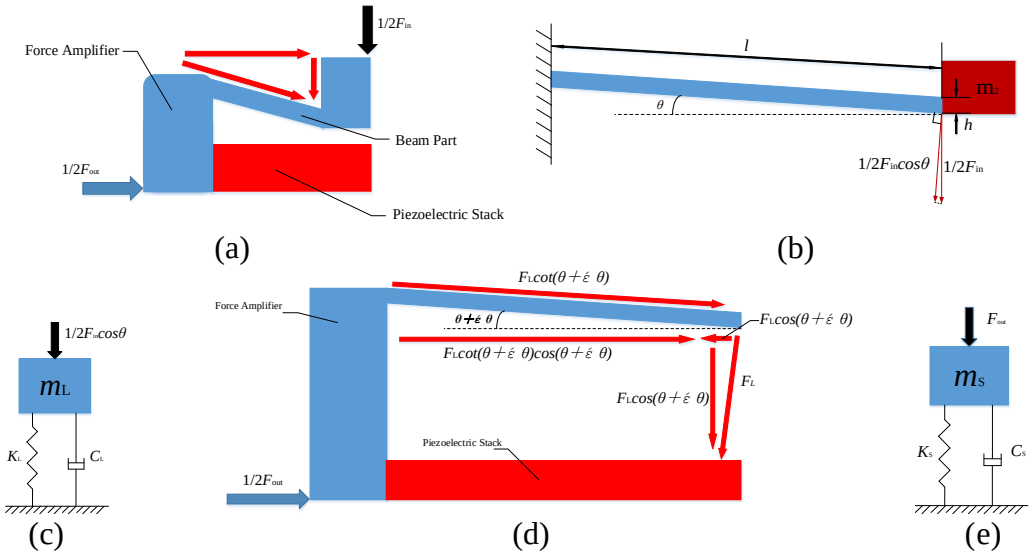

Figure 3. A model of the force amplifier: (a) a quarter model of the force amplifier; (b) a beam part of the force amplifier; (c) an equivalent spring-mass system of the beam part; (d) an elastic excitation working on the piezoelectric stack; and (e) an equivalent spring-mass system of the piezoelectric stack

For convenience and brevity, we introduce the following parameters

$$2n = \frac{C_L}{m_L},\ p^2 = \frac{K_L}{m_L},\quad q = \frac{F_{in}cos\theta}{2m_L} \tag{3}$$

Based on the classical vibration theory, the solution of Eq. (2) can be written as

$$x = Bsin(\omega t - \varphi) \tag{4}$$

where B and φ denote the amplitude and phase, respectively. Substituting Eq. (4) into Eq. (1), one gets

$$B = \frac{q}{\sqrt{(p^2-\omega^2)^2+4n^2\omega^2}} \tag{5}$$

$$\varphi = arctan(\frac{2n\omega}{p^2-\omega^2}) \tag{6}$$

Furthermore, the elastic excitation of the beam end acts on the piezoelectric stack can be obtained as

$$F_L = K_L x \tag{7}$$

In Figure 3(d), according to Newton's law, the excitation force F_{out} acting on the piezoelectric stack is

$$F_{out} = 2F_L[\cos(\theta + \Delta\theta)\cot(\theta + \Delta\theta) - \sin(\theta + \Delta\theta)] \tag{8}$$

where $\Delta\theta$ is the angular variation caused by the elastic deformation. Consider $\Delta\theta \ll \theta$, the expression of F_{out} can be re-written as

$$F_{out} = 2F_L[cos\,\theta\,cot\,\theta - sin\theta] \tag{9}$$

Hence, the amplification factor of the force amplifier is given by

$$M = \frac{F_{out}}{F_{in}} \tag{10}$$

2.2.2 Electromechanical coupling equations

From the perspective of elastic deformation, the deformation of the piezoelectric stack in the horizontal direction (the direction is perpendicular to pressure fluctuations) when subjected to positive pressure is much larger than the deformation in the vertical direction (the direction is along pressure fluctuations). The piezoelectric stack can produce a compression force under the action of positive pressure, and most of the voltage outputs are generated by the piezoelectric effect, i.e., the piezoelectric constant d_{33} in Eq. (12). To obtain the electromechanical coupling equation of the enhanced PFEH, the piezoelectric stack is regarded as a single degree-of-freedom system, see Figure 3(e). As aforementioned, the dynamic equation of the piezoelectric stack under the excitation force F_{out} can be expressed as

$$m_S\ddot{y} + C_S\dot{y} + K_S y = F_{out} \tag{11}$$

in which y is the longitudinal vibration displacement of the piezoelectric stack, C_s is a damping coefficient of the system, $m_S = \frac{N\rho dS}{3}$ and $K_S = NE_S d$ are the equivalent mass and stiffness of piezoelectric stack, respectively. In addition, the parameters N, d and S are the number, thickness and area of the piezoelectric sheets, respectively. ρ and E_S are

the density and elastic modulus of the piezoelectric materials, respectively.

Since the piezoelectric stack can only produce vibration in the longitudinal direction, the piezoelectric constitutive equations are written as

$$\begin{cases} S_3 = s_{33}^E T_3 + d_{33} E_3 \\ D_3 = \varepsilon_{33}^T E_3 + d_{33} T_3 \end{cases} \tag{12}$$

Here, s_{33}^E is the flexibility of piezoelectric materials, d_{33} is the piezoelectric constant, ε_{33}^T is the dielectric constant, T_3 is the stress of piezoelectric materials, E_3 is the electric field of piezoelectric materials, S_3 is the strain of piezoelectric materials, and D_3 is the electric displacement of piezoelectric materials.

Assume that electric fields are uniformly distributed along the thickness of the piezoelectric sheets, we have

$$E_3 = \frac{V(t)}{d_1} \tag{13}$$

where $V(t)$ is the open-circuit voltage of the piezoelectric sheets. According to Eq. (12), the stress of the piezoelectric sheets under external excitations and electric fields can be obtained. Using Hooke's law, the stress of the piezoelectric sheets only under excitation $T_{3,np}$ can be obtained. Hence, the stress of the piezoelectric sheets (T_3) caused by electric fields can be expressed as

$$T_{3,p} = \frac{S_3 - d_{33}E_3}{s_{33}^E},\ T_{3,np} = \frac{S_3}{s_{33}^E},\ T_3 = T_{3,p} - T_{3,np} = -\frac{d_{33}E_3}{s_{33}^E} \tag{14}$$

Under an inverse piezoelectric effect (i.e., F_{in} = 0), the strain of the piezoelectric materials is

$$S_3 = 0 \tag{15}$$

By using Eqs. (12) and (14), the electric displacement at the upper surface of the piezoelectric layer is expressed as

$$D_3 = (\varepsilon_{33}^T - \frac{{d_{33}}^2}{s_{33}^E}) E_3 \tag{16}$$

Moreover, the electric charge ($Q(t)$) is obtained by integrating the electric displacement over the electrode area, *A*.

$$Q(t) = \int_A D_3 dA = A(\varepsilon_{33}^T - \frac{{d_{33}}^2}{s_{33}^E}) E_3 = CV(t) \tag{17}$$

Coupling with Eq. (13), the capacitance of the piezoelectric sheets is

$$C = \frac{A}{d_1}\left(\varepsilon_{33}^{T} - \frac{{d_{33}}^2}{s_{33}^{E}}\right) \tag{18}$$

In the direct piezoelectric effect (E_3 = 0), the strain of the piezoelectric materials is

$$S_3 = \frac{y}{Nd} \tag{19}$$

Making use of Eqs. (12), (14) and (18), the electric displacement at the upper surface of the piezoelectric layer is given by

$$D_3 = \frac{d_{33}}{s_{33}^{E}} S_3 \tag{20}$$

The electric charge of the piezoelectric layer are obtained as

$$Q(t) = Ad_{33}T_{3,np} = \frac{Ad_{33}S_3}{s_{33}^{E}} \tag{21}$$

Finally, the open circuit voltage of the enhanced PFEH with a parallel mode of the piezoelectric stack is derived as

$$V(t) = \frac{Q(t)}{C} = \frac{d_1 d_{33} S_3}{s_{33}^{E}\varepsilon_{33}^{T} - {d_{33}}^2} \tag{22}$$

2.3 Numerical simulations

The critical parameters for simulation are given in Table 1. Based on the above analysis, the amplification factor and the open-circuit voltage are presented in Figure 4, where "FA" represents the force amplifier. It is clear that the amplitude of the open-circuit voltage generated by adding the force amplifier is significantly higher than that of the ordinary piezoelectric stack under the same external excitation force. Because of the phase difference, the amplification factor is not constant, but it is a function of the pressure fluctuation around a constant value. Here, the constant value can be regarded as a magnification coefficient.

Table 1. Initial simulation data

Parameter	Value
h (mm)	0.3
l (mm)	14
b (mm)	5
d (mm)	1
θ (°)	6
F_0 (N)	0.25
E_L (Pa)	2×10^{11}
E_S (Pa)	1.15×10^{11}
m_L (g)	0.98

m_s (g)	3.53
A (mm^2)	25
d_{33}	2.7×10^{-10}
S_{33}	16×10^{-12}
ε_{33}	1.04×10^{-9}
C_L	0.02
C_S	0.02
N	9

Figure 5 shows the numerical results of the amplitude-frequency response curves for the magnification coefficient and the output voltage. We found that the magnification coefficient reaches a maximum value at 578.12 Hz. At the same time, the output voltage can arrive to the peak value. In fact, this is the fundamental resonance frequency of the piezoelectric stack. Based on the results, it implies that the force amplifier can improve the transformation of vibration energy.

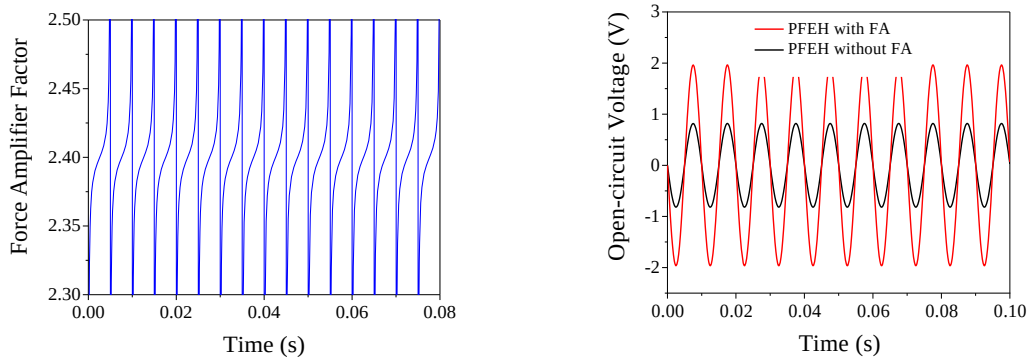

(a) (b)

Figure 4. (a) Amplification factors of the force amplifier; (b) Open-circuit voltage responses of the enhanced PFEH (comparison between two cases).

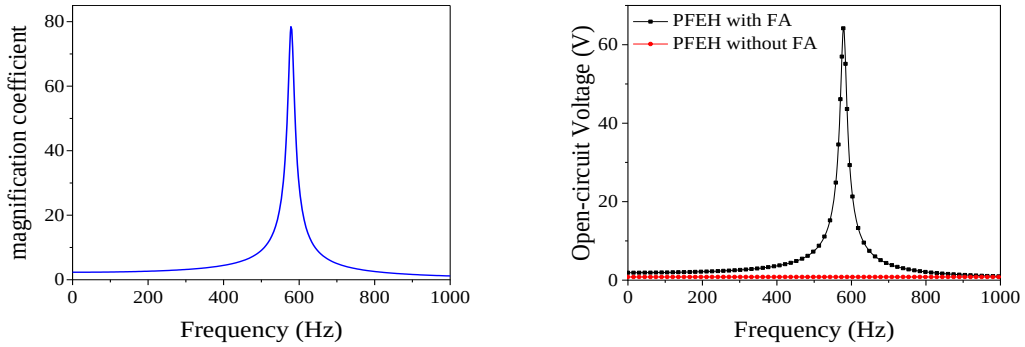

(a) (b)

Figure 5. Amplitude-frequency responses of (a) the magnification coefficient; and (b) the output voltage

To obtain the optimal parameters of the enhanced PFEH, it is necessary to study the influence of the thickness, length and structural angle of the beam parts on open-circuit voltage. In Figure 6(a), the natural frequency of the system decreases gradually with the increase of the length of the beam parts (simply termed as “beam length”). The shorter the beam length is, the higher the open-circuit voltage can be generated during resonance. Under the low-frequency and non-resonance conditions, increasing the beam length can effectively improve the open-circuit voltage output. In Figure 6(b), we observe that there exists a specific beam length that can maximize the open-circuit voltage output of the piezoelectric stack under the external excitation at different frequencies. As the frequency of external excitation increases, the specific beam length becomes shorter and the maximum open-circuit voltage output of the piezoelectric becomes higher.

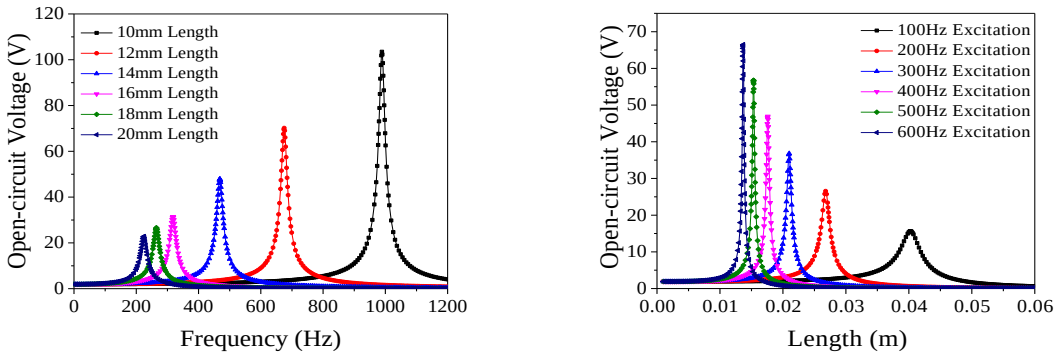

(a) (b)

Figure 6. Open-circuit voltage under (a) different lengths of the beam parts and (b) different excitation frequencies

Figure 7 shows the open-circuit voltage responses under various beam thicknesses and excitation frequencies. With the decrease of the beam thickness, the natural frequency of the system decreases gradually. The thicker the beam thickness is, the higher the open-circuit voltage can be generated during resonance. Under the low-frequency and non-resonance conditions, decreasing the beam thickness can effectively improve the open-circuit voltage output. In Figure 7(b), we observe that the beam thickness can maximize the open-circuit voltage output of the piezoelectric stack under the action of external excitations at different frequencies. When the frequency of external excitation increases, the specific beam thickness becomes thicker and the maximum open-circuit voltage output of the piezoelectric tends to be higher.

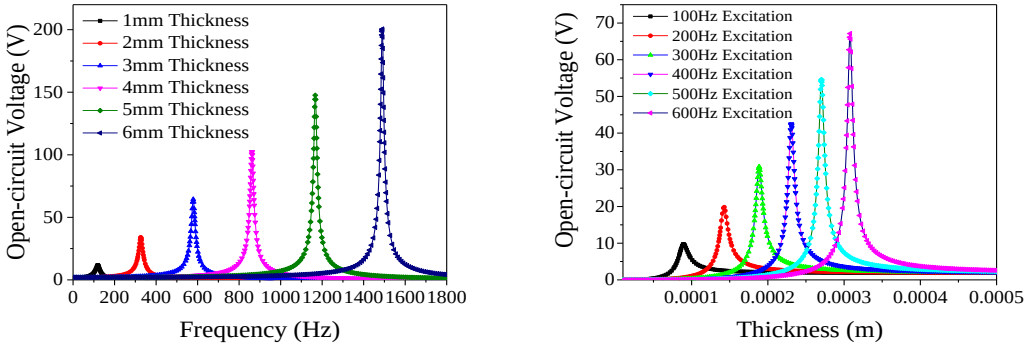

(a) (b)

Figure 7. Open-circuit voltage amplitude-frequency response curves under (a) different beam thickness dimensions; and (b) different external excitation frequencies

In Figure 8, the structural angle of the beam parts will not affect the natural frequency of the system. With the decrease of the structural angle, the open-circuit voltage of the piezoelectric stack increases gradually. Theoretically, when the structural angle is zero, the amplification factor of the system tends to be infinite, and the open circuit voltage generated by the piezoelectric stack will also be infinite. In fact, the deflection of the structural angle $\Delta\theta$ caused by the external excitation makes it impossible for this phenomenon to occur. Under the low-frequency and non-resonance conditions, the beam parts with a smaller angle can make the piezoelectric stack achieve a higher open-circuit voltage output.

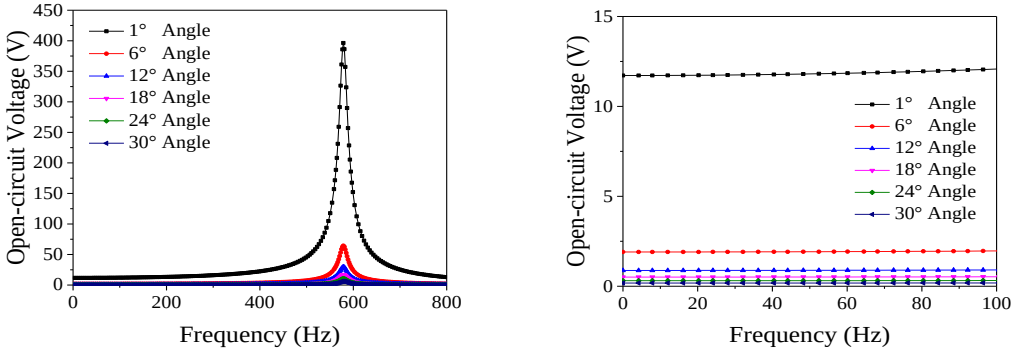

(a) (b)

Figure 8 Open-circuit voltage amplitude-frequency response curves of the piezoelectric stack with a force amplifier under various structural angles

Based on the above analysis, to improve the energy harvesting efficiency of enhanced PFEH at a low-frequency vibration environment, we found that smaller structural angle, longer and thinner beam parts should be selected. For the proposed PFEH model, we obtain a better output open-circuit voltage when the PFEH works at a resonant frequency range.

3. Finite Element Analysis

In order to verify the correctness of the theoretical analysis, a finite element model of the piezoelectric stack with the force amplifier is built in this section, as shown in Figure 9. Here, d is the beam thickness, l is the beam length, θ is the angle of each of the four beams with respect to the horizontal direction, L is the distance between the contact surfaces, H is the height of the force amplifier, and W is the width of the force amplifier. A simplified model of the piezoelectric stack, consisted of 9 piezoelectric ceramic layers, 10 copper guided layers and 2 contact parts, is considered. One end of the mechanical amplifier is fixed and the other end is subjected to an external excitation. The dimensions and material properties of the present device are presented in Tables 2 and 3, respectively.

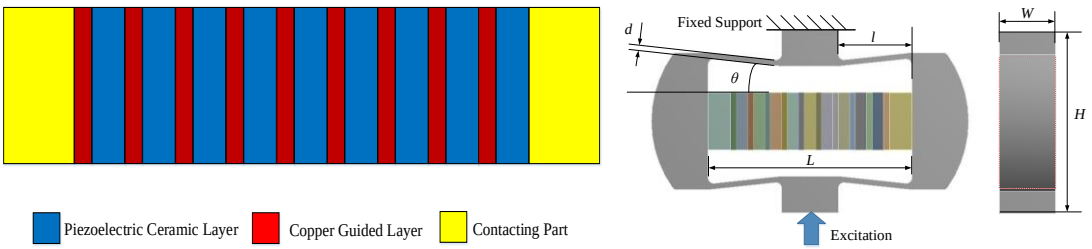

(a) (b)

Figure 9. Finite element model of (a) the piezoelectric stack; and (b) the force amplifier

Table 2. Materials and dimensions of the enhanced PFEH

	Material	Length (mm)	Wide (mm)	Height (mm)
Piezoelectric ceramic layer	PZT-5H	5	5	1
Copper guided layer	Copper alloy	5	5	0.5
Contact part	Structure steel	5	5	2

Table 3. Materials properties of the enhanced PFEH

Material	Density (kg m^{-3})	Young's Modulus (Pa)	Piezoelectric constant (Pc N^{-1})
PZT-5H	7600	1.15×10^{11}	660
Copper alloy	8300	1.1×10^{11}	———
Structural steel	7850	2×10^{11}	———

Since this work is mainly to investigate the open circuit voltage of the proposed

harvester for dynamic characterization, no load resistors are added in the finite element simulations. The effect of the mechanical amplifier on the energy harvesting efficiency is determined by comparing the open circuit voltage output of the energy trap. Figure 10 shows the finite element results, the open-circuit voltage and amplitude-frequency responses of the enhanced PFEH under various parameters (i.e., length, thickness and structural angle of the beam parts) are presented. We found that it is mostly consistent with the theoretical analysis, although there are few quantitative differences. For the enhanced PFEH under different beam thickness values, the open-circuit voltage output of the piezoelectric stack is irregular under a resonant condition with the increase of beam thickness. Under the effect of various structural angles, the natural frequency of the piezoelectric stack with the force amplifier would decrease as the structural angle decreases. When the structure angle is zero, the voltage output is the lowest under a low-frequency excitation.

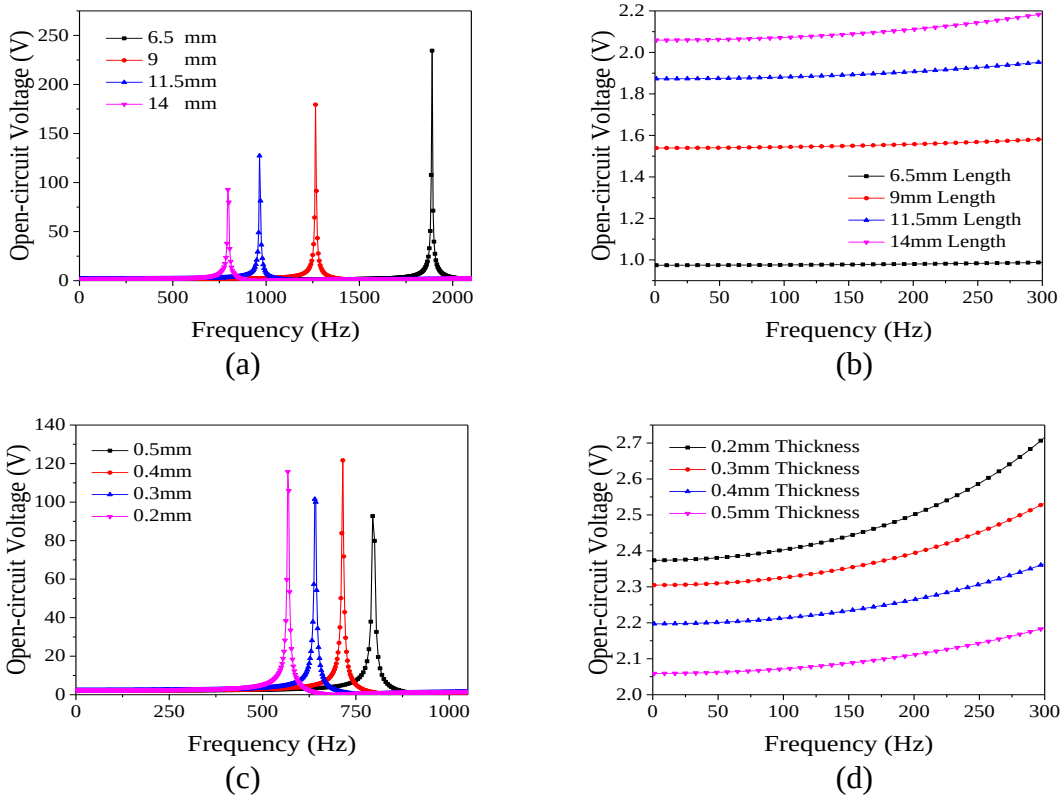

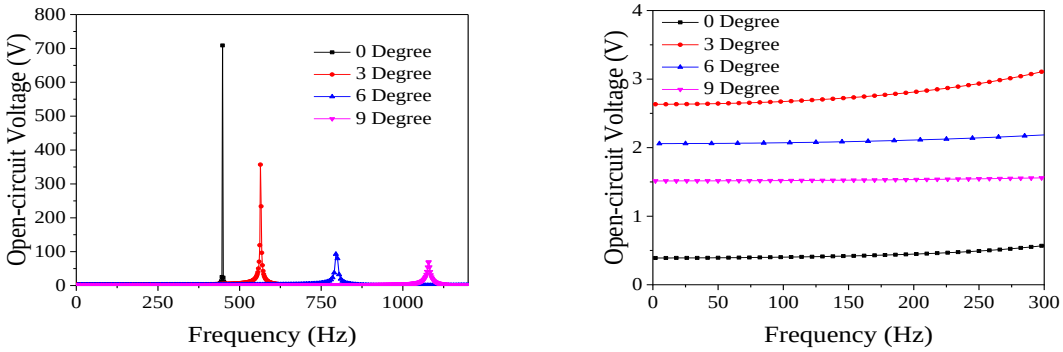

Figure 10. Open-circuit voltage amplitude-frequency responses of the enhanced PFEH with the force amplifier under the effects of (a, b) beam length; (c, d) beam thickness; and (e, f) structural angle.

Discrepancies between the finite element and dynamic models are mainly caused by the model assumptions. The model can be considered as a fully symmetrical structure only if it is subjected to either static pressure or low-frequency. As one end of the mechanical amplifier is fixed and the other end is subjected to pressure fluctuations, the structure can be divided into 4 beam sections that can move asynchronously under high-frequency vibration. In Figure 11, the effects of low-frequency and high-frequency vibrations of the model can be observed more intuitively through the finite element analysis.

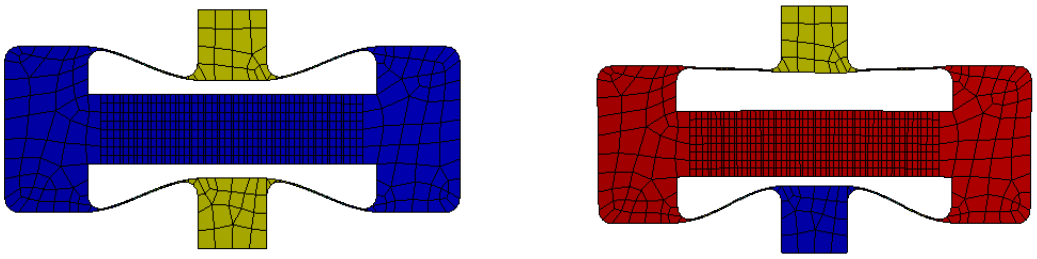

Figure 11. Deformation of the force amplifier under (a) low-frequency vibration; and (b) high-frequency vibration.

Despite there are some deviations between the analytical solutions and the finite element simulation results, the structural optimization method of the force amplifier is still consistent with the theoretical analysis. To demonstrate the benefits of the force amplifier, three cases of the enhanced PFEH, they are (i) only the piezoelectric stack (PS); (ii) the piezoelectric stack with a force amplifier (PS with FA); and the piezoelectric stack with an

optimized force amplifier (PS with OFA), are compared and discussed based on the finite element analysis. In Table 4, the detailed geometric parameters of the structure are given.

Table 4. Dimensions of three cases of the enhanced PFEH

Dimension	PS	PFEH with FA	PFEH with OFA
d (mm)	--	0.5	0.3
l (mm)	--	6.5	14
θ (°)	--	6	6
e	--	18	33
H (mm)	--	14	14
W (mm)	--	5	5

As a result, the time-history and frequency-spectrum responses of the open-circuit voltage results for these three cases are shown in Figure 12. For simulations, the static pressure, amplitude and frequency of pressure fluctuations are defined as 200 kPa, 10 kPa and 100 Hz, respectively. To give a more explicit comparison, the identified maximum values of the three cases are summarized in Table 5. It is clear that the piezoelectric stack with the force amplifier can effectively improve the RMS open-circuit voltage output. The optimized force amplifier can further increase the open-circuit voltage output among other two cases, it is approximately 8 times better than the case with the piezoelectric stack only.

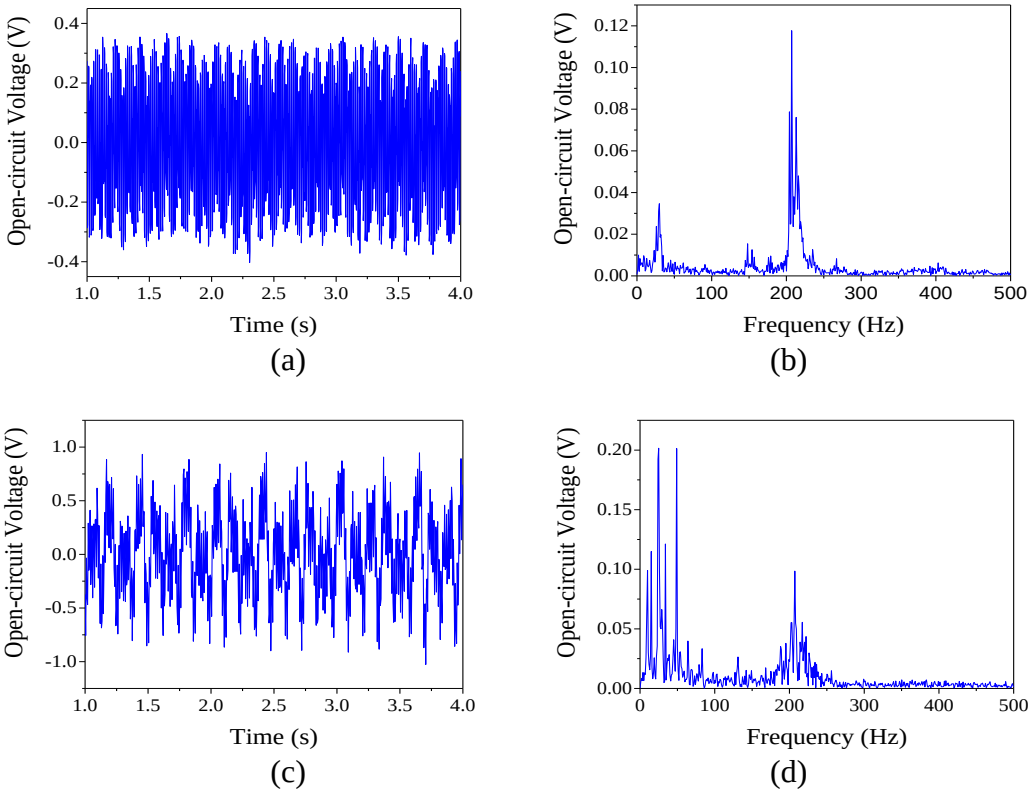

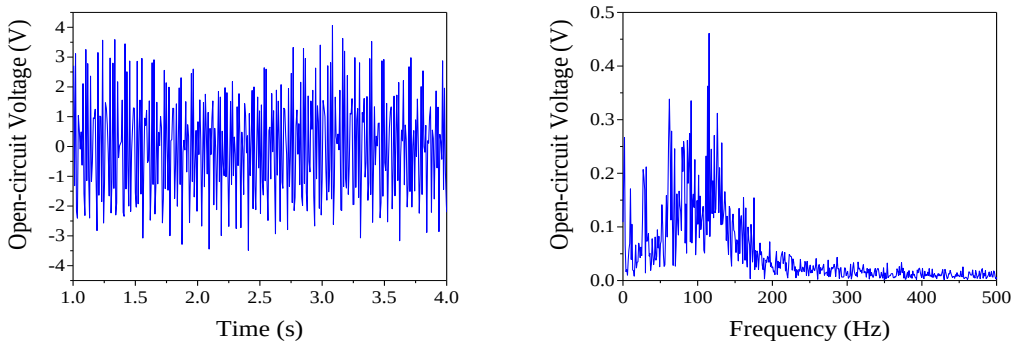

(e) (f)

Figure 12. Time-history and frequency-spectrum responses of the open-circuit voltage results for (a, b) PS; (c, d) PS with FA; and (e, f) PS with OFA.

Table 5. Identified results of three cases of the enhanced PFEH

e	PS	PFEH with FA	PFEH with OFA
Max amplitude of pressure fluctuation (kPa)	10.614	6.614	9.544
Main frequency of pressure fluctuation (Hz)	210.04	24.06	93.19
RMS open-circuit voltage output (mV)	10.311	22.972	83.622

4. Experimental Studies

In this section, an experimental platform for the enhanced PFEH resting on a hydraulic pressure pipeline system is built, as shown in Figure 13. The open-circuit voltage output of the piezoelectric stack without connecting any load resistance under pressure fluctuations can be directly measured. The time-domain and frequency-spectrum curves are plotted in Fig. 14. It is seen that the voltage output frequency of the piezoelectric stack under pressure ripples is at 47 Hz, 50 Hz and 100 Hz.

According to the above analysis, three cases of the PFEH structure are considered, i.e., the force amplifier with an optimized length (OLFA), the force amplifier with an optimized thickness (OTFA) and the force amplifier with an optimized angle (OAFA). The results are compared with two un-optimized cases. Figure 15 demonstrates the frequency-spectrum results of the open-voltage output. We observe that there are mainly three different pressure pulsation frequencies in the hydraulic pressure pipeline, i.e., 47 Hz, 50 Hz and 100 Hz. Table 6 shows the peak value of the voltage at various frequencies. It is found that the implementation of an un-optimized FA for the PFEH results in a decrease of the voltage. However, the voltage can be significantly increased by increasing the length and reducing

the thickness and structure angle of the beam parts.

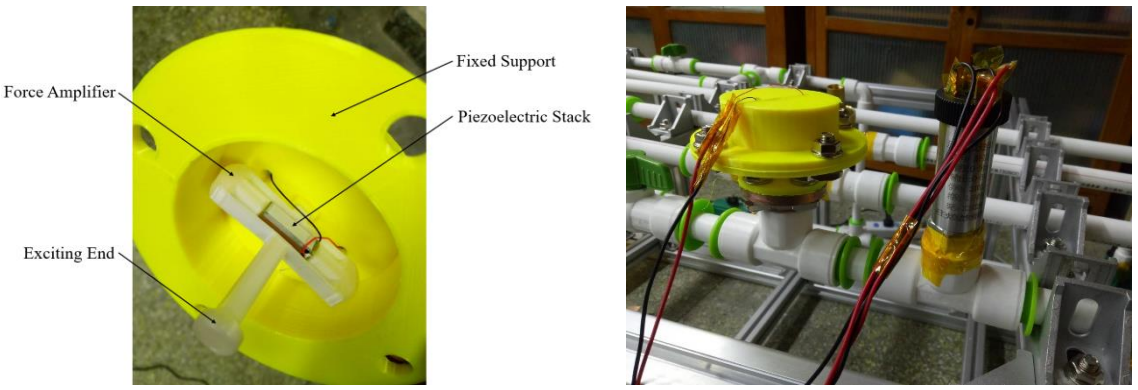

(a) (b)

Figure13 Experimental platform of the PFEH (a) Piezoelectric stack with force amplifier; and (b) Pressure detection device and energy harvester

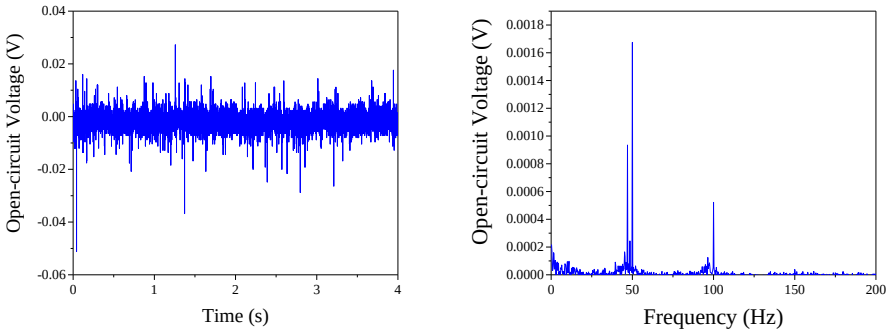

(a) (b)

Figure 14. Voltage output responses for (a) time-domain; and (b) frequency-spectrum analysis

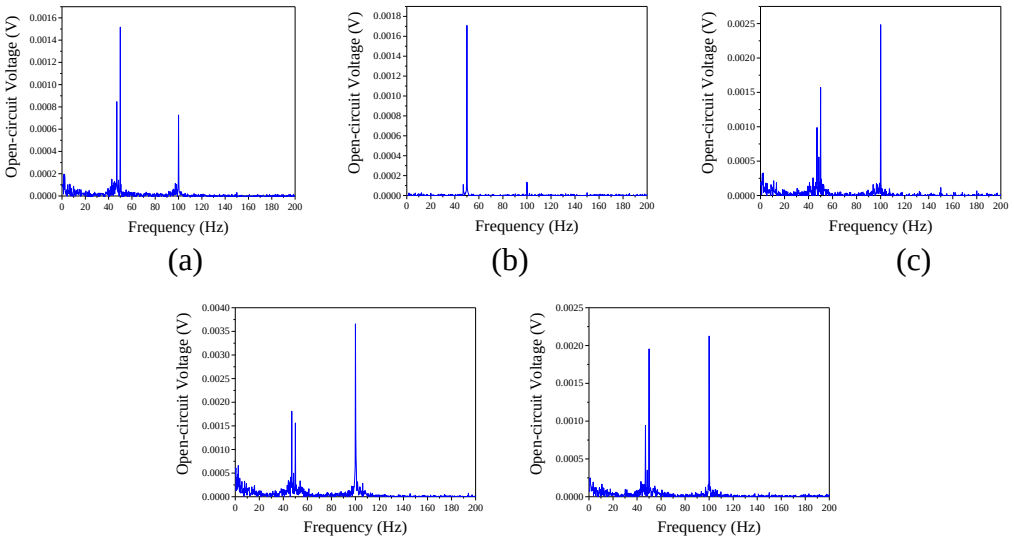

(a) (b) (c)

(d) (e)

Figure 15. Open-voltage output curves for (a) PS; (b) PS with FA; (c) PS with OLFA; (d) PS with OTFA; and (e) PS with OAFA

Table 6. Open-voltage outputs under various frequencies of pressure fluctuations of PS, PS with FA, OLFA, OTFA and OAFA

	47 Hz (mV)	50 Hz (mV)	100 Hz (mV)	RMS (mV)
PS	0.88	1.54	0.65	1.10
PS with FA	0.12	1.72	0.13	1.00
OLFA	0.95	1.59	2.52	1.81
OTFA	1.97	1.61	3.73	2.60
OAFA	0.98	1.91	2.10	1.73

In essence, the natural frequency of the system can be reduced by increasing the beam length and reducing the thickness and structural angle of the beam part. When the natural frequency of the system approaches to 100 Hz, a resonance phenomenon will occur. This will increase the open-circuit voltage output under pressure fluctuations at 100 Hz. When the natural frequency of the system is lower than 100 Hz, no resonance phenomenon will appear. This will reduce the open-circuit voltage output under pressure fluctuations at 100 Hz and increase the open-circuit voltage output under pressure fluctuations at 50 Hz. The experimental results show the advantages of the optimized force amplifier for the enhanced PFEH, it implies that the energy conversion efficiency can be effectively improved by optimizing the force amplifier structure.

5. Conclusions

In this work, coupling a piezoelectric stack with a force amplifier for energy harvesting from a hydraulic pressure pipeline system under low-frequency excitation levels is designed and analyzed. The working principle of the force amplifier is explained by using a dynamic model. It is found that the force amplifier possesses the function of magnifying external excitations that act on the piezoelectric stack. Moreover, to obtain higher output voltages of the enhanced PFEH, it is found that the structural angle and the beam dimensions are the critical parameters to optimize the effect of the force amplifier. The analytical solutions are verified by the finite element and experimental results. The force amplifier deployed on the piezoelectric stack can effectively increase the RMS open-circuit voltage output. Moreover, the optimized force amplifier can further improve the performance of the enhanced PFEH. In general, the flow rate of pipeline systems can affect the performance of such a device. A

higher dynamic pressure in pipelines will increase both flow rate and pressure fluctuations, this will further induce a higher voltage output of the current device. We also realized that the contact area between the energy trap and the hydraulic pipe is another important factor that can affect the efficiency of energy harvesting. Based on the current work, the contact area is 50.24 mm^2, we estimated that the output density of the open circuit voltage is about 517 V/m^2. This is a favorable result for energy harvesting applications. Since pressure fluctuations occur everywhere in pipeline systems, it is expected that the voltage output can be effectively improved by enlarging the contact area. On the basis of this work, local pressure fluctuations under the flow-induced vibration effect can improve the energy harvesting efficiency. The present study shows that the proposed PFEH has great potential as a self-powered technique to support low-power wireless sensor networks for intelligent monitoring in pipeline systems.

Acknowledgments

The authors gratefully acknowledge the support of the National Natural Science Foundation of China (Grant Nos.11672008, 11972051 and 11832002). The last author (S.K. Lai) would like to acknowledge the financial support provided from the Early Career Scheme of the Hong Kong Research Grants Council (Project No. PolyU 252026/16E).

Declaration of conflicting interests

On behalf of all authors, the corresponding author states that there is no conflict of interest.

References

[1] Zhang, Y.L., Wang, T.Y., Zhang, A., Peng, Z.T., Luo, D., Chen, R., et al. (2016), "Electrostatic energy harvesting device with dual resonant structure for wideband random vibration sources at low frequency", *Rev Sci Instrum*, **87**(12), 125001.

[2] Lallart, M., Wang, L. and Petit, L. (2016), "Enhancement of electrostatic energy harvesting using self-similar capacitor patterns", *Journal of Intelligent Material Systems & Structures*, **27**(17), 2385-2394.

[3] Perez, M., Boisseau, S., Gasnier, P., Willemin, J., Geisler, M. and Reboud, J.L. (2016), "A cm scale electret-based electrostatic wind turbine for low-speed energy harvesting applications", *Smart Mater Struct*, **25**(4), 045015.

[4] Morgado, M.L., Morgado, L.F., Silva, N. and Morais, R. (2015), "Mathematical modelling of cylindrical electromagnetic vibration energy harvesters", *International Journal of Computer Mathematics*, **92**(1), 101-109.

[5] Moss, S.D., Payne, O.R., Hart, G.A. and Ung, C. (2015), "Scaling and power density metrics of electromagnetic vibration energy harvesting devices", *Smart Mater Struct*, **24**(2), 023001.

[6] Zhang, Y., Cao, J.Y., Zhu, H.Y. and Lei, Y.G. (2019), "Design, modeling and experimental verification of circular Halbach electromagnetic energy harvesting from bearing motion", *Energy Convers Manage*, **180**, 811-821.

[7] Erturk, A. and Inman, D.J., Piezoelectric energy harvesting, Chichester: Wiley; 2011.

[8] Cao, D.X., Guo, X.Y. and Hu, W.H. (2019), "A novel low-frequency broadband piezoelectric energy harvester combined with a negative stiffness vibration isolator", *J Intell Mater Syst Struct*, **30**(7), 1105-1114.

[9] Li, X., Zhang, Y.W., Ding, H. and Chen, L.Q. (2017), "Integration of a nonlinear energy sink and a piezoelectric energy harvester", *Appl Math Mech-Engl Ed*, **38**(7), 1019-1030.

[10] Yao, M.H., Zhang, W. and Yao, Z.G. (2015), "Nonlinear Vibrations and Chaotic Dynamics of the Laminated Composite Piezoelectric Beam", *J Vib Acoust-Trans ASME*, **137**(1), 011002.

[11] Cao, D., Xia, W. and Hu, W. (2019), "Low-frequency and broadband vibration energy harvester driven by mechanical impact based on layer-separated piezoelectric beam", *Applied Mathematics and Mechanics (English Edition)*, **40**(12), 1777-1790.

[12] Zhang, X.Q., Pondrom, P., Sessler, G.M. and Ma, X.C. (2018), "Ferroelectret nanogenerator with large transverse piezoelectric activity", *Nano Energy*, **50**, 52-61.

[13] Zhu, R.J., Wang, Z.M., Ma, H., Yuan, G.L., Wang, F.X., Cheng, Z.X., et al. (2018), "Poling-free energy harvesters based on robust self-poled ferroelectric fibers", *Nano Energy*, **50**, 97-105.

[14] Anton, S.R., Farinholt, K.M. and Erturk, A. (2014), "Piezoelectret foam-based vibration energy harvesting", *J Intell Mater Syst Struct*, **25**(14), 1681-1692.

[15] Erturk, A. and Inman, D.J. (2009), "An experimentally validated bimorph cantilever model for piezoelectric energy harvesting from base excitations", *Smart Mater Struct*, **18**(2), 025009.

[16] Erturk, A., Hoffmann, J. and Inman, D.J. (2009), "A piezomagnetoelastic structure for broadband vibration energy harvesting", *Appl Phys Lett*, **94**(25), 254102.

[17] Sun, S. and Cao, S.Q. (2017), "Analysis of chaos behaviors of a bistable piezoelectric cantilever power generation system by the second-order Melnikov function", *Acta Mech Sin*, **33**(1), 200-207.

[18] Lan, C.B., Qin, W.Y. and Deng, W.Z. (2015), "Energy harvesting by dynamic unstability and

internal resonance for piezoelectric beam", *Appl Phys Lett*, **107**(9), 093902.
[19] Zhou, S.X., Cao, J.Y., Inman, D.J., Lin, J., Liu, S.S. and Wang, Z.Z. (2014), "Broadband tristable energy harvester: Modeling and experiment verification", *Appl Energy*, **133**, 33-39.
[20] Zhou, S.X. and Zuo, L. (2018), "Nonlinear dynamic analysis of asymmetric tristable energy harvesters for enhanced energy harvesting", *Commun Nonlinear Sci Numer Simul*, **61**, 271-284.
[21] Lai, S.K., Wang, C. and Zhang, L.H. (2019), "A nonlinear multi-stable piezomagnetoelastic harvester array for low-intensity, low-frequency, and broadband vibrations", *Mech Syst Sig Process*, **122**, 87-102.
[22] Liu, F.R., Zou, H.X., Zhang, W.M., Peng, Z.K. and Meng, G. (2018), "Y-type three-blade bluff body for wind energy harvesting", *Appl Phys Lett*, **112**(23), 233903.
[23] Yuan, T.C., Yang, J. and Chen, L.Q. (2018), "Nonlinear dynamics of a circular piezoelectric plate for vibratory energy harvesting", *Commun Nonlinear Sci Numer Simul*, **59**, 651-656.
[24] Zhao, L.C., Zou, H.X., Yan, G., Zhang, W.M., Peng, Z.K. and Meng, G. (2018), "Arbitrary-directional broadband vibration energy harvesting using magnetically coupled flextensional transducers", *Smart Mater Struct*, **27**(9), 095010.
[25] Fan, K.Q., Cai, M.L., Wang, F., Tang, L.H., Liang, J.R., Wu, Y.P., et al. (2019), "A string-suspended and driven rotor for efficient ultra-low frequency mechanical energy harvesting", *Energy Convers Manage*, **198**, 111820.
[26] Liu, D., Xu, Y. and Li, J.L. (2017), "Probabilistic response analysis of nonlinear vibration energy harvesting system driven by Gaussian colored noise", *Chaos Solitons Fractals*, **104**, 806-812.
[27] Liu, D., Xu, Y. and Li, J.L. (2017), "Randomly-disordered-periodic-induced chaos in a piezoelectric vibration energy harvester system with fractional-order physical properties", *J Sound Vib*, **399**, 182-196.
[28] Lu, Z.Q., Ding, H. and Chen, L.Q. (2019), "Resonance response interaction without internal resonance in vibratory energy harvesting", *Mech Syst Sig Process*, **121**, 767-776.
[29] Cao, D.X., Leadenham, S. and Erturk, A. (2015), "Internal resonance for nonlinear vibration energy harvesting", *Eur Phys J-Spec Top*, **224**(14-15), 2867-2880.
[30] Chen, L.Q. and Jiang, W.A. (2015), "Internal Resonance Energy Harvesting", *J Appl Mech-Trans ASME*, **82**(3), 031004.
[31] Jiang, W.A., Chen, L.Q. and Ding, H. (2016), "Internal resonance in axially loaded beam energy harvesters with an oscillator to enhance the bandwidth", *Nonlinear Dyn*, **85**(4), 2507-2520.
[32] Shoele, K. and Mittal, R. (2016), "Energy harvesting by flow-induced flutter in a simple model of an inverted piezoelectric flag", *J Fluid Mech*, **790**, 582-606.
[33] Song, R.J., Shan, X.B. and Xie, T. (2016), "Numerical Study of the Aerodynamic Response and Energy Harvesting of Polyvinylidene Fluoride Piezoelectric Flags in a Uniform Flow", *J Chin Chem Soc*, **63**(6), 545-552.
[34] Cunefare, K.A., Skow, E.A., Erturk, A., Savor, J., Verma, N. and Cacan, M.R. (2013), "Energy harvesting from hydraulic pressure fluctuations", *Smart Materials and Structures*, **22**(2), 025036.
[35] Skow, E.A., Cunefare, K.A. and Erturk, A. (2014), "Power performance improvements for high pressure ripple energy harvesting", *Smart Materials and Structures*, **23**(10), 104011.
[36] Feenstra, J., Granstrom, J. and Sodano, H. (2008), "Energy harvesting through a backpack employing a mechanically amplified piezoelectric stack", *Mechanical Systems and Signal*

Processing, **22**(3), 721-734.

[37] Chen, S.B., Wang, L.R., Zhou, W.L., Musgrave, P., Xu, T.B. and Zuo, L. (2015), "Optimal design of force magnification frame of a piezoelectric stack energy harvester", *Proc of SPIE* **9435**, 943516.

[38] Wang, Y., Chen, W. and Guzman, P. (2016), "Piezoelectric stack energy harvesting with a force amplification frame: Modeling and experiment", *J Intell Mater Syst Struct*, **27**(17), 2324-2332.

[39] Kuang, Y., Daniels, A. and Zhu, M. (2017), "A sandwiched piezoelectric transducer with flex end-caps for energy harvesting in large force environments", *J Phys D: Appl Phys*, **50**(34), 345501.

[40] Qian, F., Xu, T.-B. and Zuo, L. (2018), "Design, optimization, modeling and testing of a piezoelectric footwear energy harvester", *Energy Convers Manage*, **171**, 1352-1364.

[41] Evans, M., Tang, L. and Aw, K.C. (2018), "Modelling and optimisation of a force amplification energy harvester", *J Intell Mater Syst Struct*, **29**(9), 1941-1952.

[42] Keshmiri, A., Deng, X. and Wu, N. (2019), "New energy harvester with embedded piezoelectric stacks", *Composites Part B-engineering*, **163**, 303-313.

[43] Duan, X. and Cao, D. (2019), "Low-frequency resonant vibration energy harvester using piezoelectric stacks with force magnification frames", *IOP Conference Series: Materials Science and Engineering*, Suzhou, China, September.